Studies of a modulated Hall thruster

IOP Publishing Plasma Sources Science and Technology
Plasma Sources Sci. Technol. **XX** (XXXX) XXXXXX https://doi.org/XXXX/XXXX

Studies of a modulated Hall thruster

Jacob Simmonds[1], Yevgeny Raitses[1] Andrei Smolyakov[2], and Oleksandr Chapurin[2]

[1] Princeton Plasma Physics Laboratory, Princeton, NJ 08543, United States of America
[2] University of Saskatchewan, Saskatoon, SK S7N5E2, Canada

E-mail: jacobbs@princeton.edu

Received xxxxxx
Accepted for publication xxxxxx
Published xxxxxx

Abstract

A typical Hall thruster is powered from a DC power supply and operates with a constant discharge voltage. In operation, the discharge current is subject to strong low frequency oscillations (so-called breathing oscillations). Recent studies have shown that not only can these breathing oscillations be correlated with improved performance, but these oscillations can be induced and controlled by modulating the anode voltage. In this work, a systematic experimental study of the plasma flow in a modulated cylindrical Hall thruster was performed to characterize the effect of natural and modulated breathing oscillations on thruster performance. Measurements suggest that modulating the anode voltage in resonance with the natural breathing frequency does increase the thrust, but a corresponding phase alignment of discharge current and discharge voltage causes the efficiency gains to be insignificant. In addition, the outward shift of the acceleration region causes the plasma plume divergence to increase at the resonance condition and thereby, limit the thrust increase. Mechanisms underlying the relative phase between discharge current, ion current, and discharge voltage are investigated experimentally and corroborated with one-dimensional hybrid simulations of the thruster discharge.

Keywords: plasma propulsion, Hall thruster, efficiency, breathing mode, oscillations control, modelling, performance, phasing

1. Introduction

Hall Thrusters, a widely used and mature technology for spacecraft propulsion, are subject to large amplitude, low frequency (up to 100% of steady state values, 10-30 kHz) discharge current oscillations, commonly known as the breathing mode [1]. This breathing mode is typically attributed to the ionization instability associated with periodic depletion of neutral gas propellant atoms in the channel. This induces oscillations of other plasma parameters including plasma density, electron temperature, plasma potential, ion energy, and ion flux. In addition to temporal changes of the plasma parameters, the breathing mode manifests itself as spatial changes of these plasma parameters in the thruster channel, propagating along the channel in an ionization front. Several models have attempted to describe the breathing mode, notably the predator-prey model by Fife *et*

al [2] and the more advanced ionization global models by Hara *et al*, which includes electron energy and loss mechanisms [3]. While useful for the identification of the ionization and neutral depletion behaviour of the breathing oscillations, these zero-dimensional models cannot capture all associated physics, specifically the propagation of the ionization front in the channel.

The amplitude and frequency of breathing oscillations are dependent on the Hall thruster operating parameters: the magnetic field, discharge voltage, and the gas flow. For low power thrusters, these oscillations can be controlled and even mitigated by enhancing the electron supply from the cathode [4]. In addition, several recent studies demonstrated that these oscillations can be induced and driven by modulating the anode voltage with an additional AC power supply placed in series with the main DC power supply [5–8]. Fig. 1 shows a typical modulation of thruster discharge voltage used in these previous studies. A key result of these studies is that the ionization of the working gas (thruster propellant) can be enhanced by modulating the anode voltage in resonance with the natural breathing frequency [9]. The maximum increase of the ion current measured in the plume occurred when oscillations of the ion density and ion velocity come into phase due to the anode voltage modulation. It was also proposed that the thrust should also increase with the resonant anode modulation due to the increased ion plume current and propellant utilization [9]. Work by Wei *et al* describes the effect of natural breathing modes on the performance of the thruster, showing correlations between increased thrust and larger discharge current oscillations [10]. Yamomato *et al* demonstrated a small performance increase with their "Volterra Engine", which allows the anode voltage to oscillate as the impedance of the thruster changes at breathing mode frequencies [11,12]. Work by Tamida *et al* demonstrated an increase up to 30% in thruster efficiency by pulsing the anode voltage at frequencies close to the natural breathing frequency, which de-phased the discharge current and discharge voltage oscillations and lowered input power [13]. In Refs. [11–13], the modulation approach was different from the work described here and no studies of these effects on plasma parameters were reported, but their approach to the design of the power supply appears to be relevant to the approach described in this paper. Finally, the ability for driven breathing oscillations to improve current efficiency was also suggested by recent work [9], where it was demonstrated that modulation of thrusters at breathing frequencies can suppress the spoke instability, which induces anomalous electron transport across magnetic fields [14].

These results support the proposed hypothesis that inducing such breathing oscillations may provide an avenue to increase thruster performance. Improvement of performance through such an alteration of operating regime would be of great benefit towards the development of Hall thruster technology, particularly in the low power regime where efficiency remains a problem. This study focuses on the application of such voltage modulations on the cylindrical geometry Hall thruster (CHT) [15].

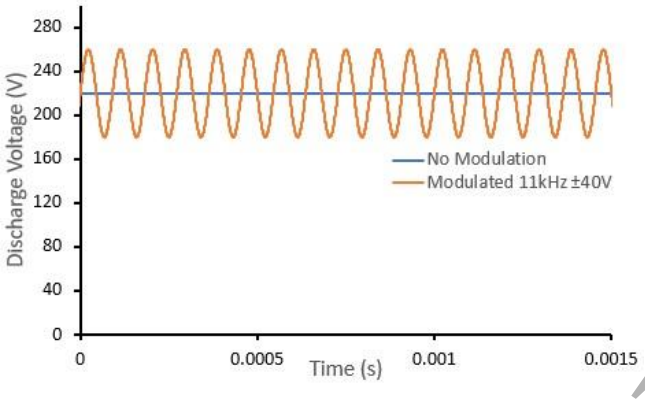

FIG. 1: A typical oscillation of the anode voltage during modulation

In Ref [16], it was shown theoretically that for a voltage modulated thruster, if the ion energy and the ion current oscillate in phase, there is an increase in the fraction of high energy ions which results in an increase of the thrust. For example, for a thruster with sinusoidally oscillating ion energy and ion current, the thrust is expressed as commonly measured plume parameters [16]:

$$Thrust = \sqrt{\frac{2M\bar{V}_i}{e}}\left(\bar{I}_i + \hat{I}_i \cos\phi_i \ \frac{\hat{V}_i}{4\bar{V}_i}\right), \tag{1}$$

where, M is the ion mass, e is charge, $\bar{V}_i \equiv \frac{\varepsilon}{e}$ (mean ion energy per charge), $\bar{I}_i$ is the mean ion current, $\hat{V}_i$ is the amplitude of the sinusoidally oscillating ion energy/charge, $\hat{I}_i$ is the amplitude of the sinusoidally oscillating ion current, and ϕ_i is the phase angle between ion current and ion energy oscillations. In the derivation of Eq. (1), the ions were assumed to be singly charged and no plume divergence was considered; a more general expression should account for multiple charged ions and plume angle. The coefficient ¼ falls out of a simplification of the expansion of the sinusoidal oscillation; the full derivation can be found in Ref. [16]. Following Eq. (1), it is then expected that for the amplitudes of the anode voltage considered in this paper ($\bar{V}_i = 220$ V; $\hat{V}_i = 40$ V; $\hat{I}_i = \hat{I}_i$), the thrust would improve by 6%, assuming the mean ion energy remains constant and full oscillations of the ion current are achieved. Similarly, the discharge power of the thruster can be expressed as:

$$P = \bar{I}_d\bar{V}_d + \hat{I}_d\hat{V}_d \cos(\phi_d)\,/2, \tag{2}$$

where $\bar{I}_d$ is mean discharge current, $\bar{V}_d$ is mean discharge voltage, $\hat{I}_d$ is the amplitude of discharge current, $\hat{V}_d$ is the amplitude of discharge voltage, and ϕ_d is the phase angle between discharge current and discharge voltage.

In this work, a permanent magnet version of the low power (100-200 W) 2.6 cm CHT was investigated. Both thrust and power were measured alongside each of these individual parameters to determine the magnitude of the thrust improvement, as well as which parameters limit further improvement. Thruster performance did not improve as anticipated, and so in an effort to understand causes for this discrepancy and to determine how the thruster plasma changes during modulation, we conducted 1D hybrid simulations of a modulating Hall thruster with input parameters and magnetic field profile corresponding the CHT. Section 2 presents an overview of the experimental diagnostics, the CHT, and the computational model used in this work. Section 3 describes the experimental results; in particular, measurements of performance and all parameters of equations (1) & (2). Section 4 discusses the results of the simulations, which predict the ionization front traveling along the channel of the modulating thruster and demonstrate how it affects the ion energy, ion current, and the resulting phasing.

2. Experimental Setup and Computational Approach

2.1. Facility and Thruster

All experiments were conducted in a small Hall thruster experimental facility described elsewhere [17]. This facility consists of a 0.4 m^3 vacuum chamber equipped with a turbomolecular pump and backed with a mechanical-blower pumping system. With a xenon flow rate of 4 sccm, this system is capable to maintain a background gas pressure in the vacuum chamber not exceeding 10^{-5} Torr. Gas flow rates were measured with a 10 sccm MKS flow controller calibrated with xenon with ±0.1 sccm uncertainty in the applied mass flow.

In previous studies [9], the effect of externally driven breathing oscillations on the thruster discharge was investigated using a 2.6cm cylindrical Hall thruster with two electromagnets and a thermionic hollow cathode [17]. In this work, we use a permanent magnet version of this thruster with the magnetic shield (Fig. 2). This thruster is described in Ref. [18] where it is referred to as the CHTpm2. With the magnetic shield, the magnetic field topology (Fig. 3) is similar to the magnetic field topology of the CHT with electromagnets [18,19]. Since this study involves thrust measurements using a high resolution and high sensitivity (±0.02 mN) thrust-stand, the choice of thruster with permanent magnets was dictated by lower operating temperatures of this thruster (≤200 °C) as compared to its electromagnet counterpart (~ 400 °C). A lower temperature of the permanent magnet CHT is due to the absence of electromagnet coil heating which can be significant for miniaturized Hall thrusters.

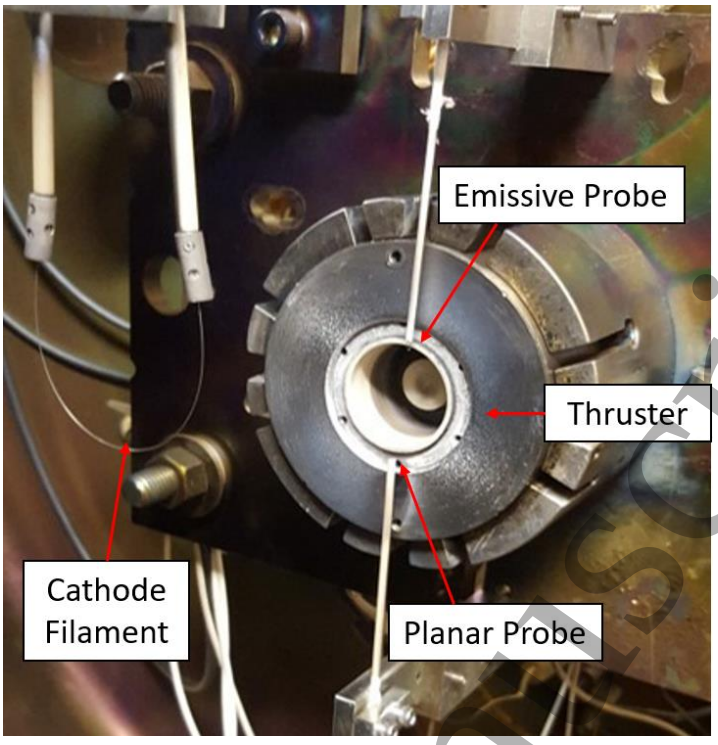

FIG. 2: 2.6cm CHTpm2 with tungsten filament cathode, planar probe and emissive probe.

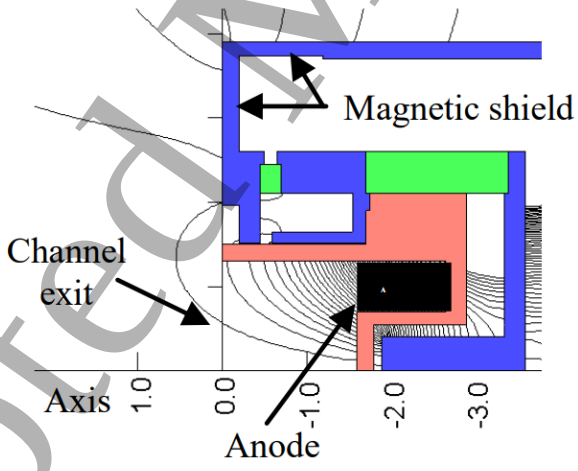

FIG. 3: Magnetic field (simulations) for the 2.6cm diameter CHT with permanent magnets and magnetic shield [18]. Blue regions comprise the magnetic core (low-carbon steel), green regions are SmCo permanent magnets, the red region is Boron Nitride, and black is the anode (non-magnetic stainless steel).

The CHTpm2 was operated with a thoriated tungsten filament as the cathode. In previous studies [20], it was already shown that the electron emission current produced by the thermionic filament is capable of sustaining a typical CHT discharge with a current of up to 1.5 A. The heating of the filament was maintained so as to achieve saturation of the discharge current (so-called "current overrun" regime [4]). In this paper, unless otherwise stated, we discuss results for the thruster operating with a discharge voltage of 220V and 40V amplitude modulations which ranged in frequency. The discharge voltage and current were measured with a digital oscilloscope at a sample rate of 2.5 MHz and a 1 Ω current shunt.

2.2. Diagnostic Setup

The following diagnostics were used in this work: planar probes to measure plasma density at the channel exit, emissive probes for plasma potential measurement at the channel exit, a movable ion flux probe for plasma plume characterization, a retarding potential analyser for the determination of the ion energy distribution function in the thruster plume, and a torsion balance thrust stand to measure the thrust and deduce the thruster performance, including specific impulse the thruster efficiency.

Plasma density, plasma potential and plume properties

The probe setup consists of several electrostatic probes to measure plasma density, plasma potential, and total ion current. A schematic of the probes can be found in Fig. 4. Ion density n_i was measured by a -40V negatively biased planar probe placed at the thruster exit (Fig. 2). The planar probe was constructed of 0.74 mm diameter tungsten wire and 1.22 mm diameter alumina tubing with the tungsten collecting surface flush with the end of the alumina tubing. The probe design has been used in previous works and further details can be found in Ref. [21]. Plasma density was deduced from the measured ion saturation current I_{is}, assuming a thin sheath [21]:

$$I_{is} = 0.61 n_i e v_B A_p = 0.61 n_i e \sqrt{T_e/M} A_p, \quad (3)$$

where I_{is} is the measured saturated ion current, n_i is the ion density, v_B is the Bohm velocity, A_p is the probe area, T_e is the electron temperature, and M is the ion mass. During breathing oscillations, the measured ion probe current oscillates too. According to Eq. (3) the probe current can oscillate due to oscillations of the plasma density or the electron temperature or both. In the present work, the electron temperature was not measured. However, assuming that the electron temperature changes proportionally to the anode voltage during modulation [22], and taking into account that the maximum voltage oscillations are

±40V (18% of the mean), we can anticipate maximum changes of the probe current due to electron temperature oscillations to not exceed ±10% of the steady state value due to the square root dependence. In contrast, both the measured probe current and discharge current oscillations may be as strong as 100% of their average values. This implies that the measured probe current oscillations are mainly due to oscillations of the plasma density. Here, we also assume that during the modulations, the planar thin sheath assumption remains valid. Therefore, the implication of the probe current oscillations as the result of the plasma density oscillations is consistent with results of simulations described in Section 4. Consequently, the relative plasma density across regimes were measured rather than the absolute values.

Oscillations of the plasma potential were measured using a floating emissive probe placed at the same channel exit location as the planar probe used for measurements of the plasma density (Fig. 4). The electric potential was measured with respect to ground. These measurements were used to monitor changes of the placement of the acceleration region – the region of high electric field in which ions receive most acceleration – with respect to the thruster exit. The difference between the anode voltage and the plasma potential measured with the probe defines the voltage potential drop inside the thruster channel and may manifest changes in the placement of the ionization and acceleration regions with respect to the channel exit.

In addition to parameters of the plasma at the channel exit, plasma plume properties including angular ion flux distribution and plume angle were deduced from the ion current measurements using a 1cm diameter planar probe biased negatively -40V with respect to ground. This probe has a guarding sleeve around the probe collector to minimize possible edge effects. Therefore, it is reasonable to expect that this probe collects the ion flux from the area determined by the probe diameter of 1 cm. The plume probe can be rotated with respect to the thruster exit ± 90°, with a distance between the probe and the thruster exit of 17 cm. This enabled measurements of the half-angle plume divergence, which is defined as half the angle at which 90% of the ion current is encompassed. The plume divergence represents a direct loss of thrust as the radial components do not contribute to the axial momentum transfer. Conventional annular geometry Hall thrusters (so-called Stationary Plasma Thrusters or SPT-type thrusters) typically have plume half-angles between 40-60º [23–25], which is high due to the existence of radial electric fields, collisions, and the inefficient placement of the ionization region [26]. CHTs operate with higher plume angles than SPTs due to their large axial magnetic fields which induces radial electric fields [27]. The exact relation between plume angle and thrust depends on the shape of the plume profile, as well as the ion velocity profile, but a first order approximation [28] is:

$$\eta_{div} = \cos\theta_{div}, \tag{4}$$

where η_{div} is the factor applied to thrust and θ_{div} is the plume half-angle. Here it is assumed ion velocity does not change with angle, as experimental measurements of ion energy on-axis and 45° off-axis found velocity to decrease by at most 5%, although more accurate measurements of the divergence factor would include this velocity-angle contribution. Plume half-angle was found by measuring the ion plume with the sweeping plume probe and calculated by:

$$0.95\left(\pi r_p^2 \int_{-\pi}^{\pi} j_i \sin\theta \, d\theta\right) = 2\pi r_p^2 \int_0^{\theta_{div}} j_i \sin\theta \, d\theta, \quad (5)$$

where r_p is the distance between the probe face and the thruster, j_i is the measured current signal, and θ is the angle of measurement from the thruster centerline. The errors associated with total ion current and plume angle measurements were found by the standard deviation of a series of measurements taken at the no modulation case. This was found to be ±0.003 A for ion current and ±0.3° for the plume angle.

As with previous experiments, measurement uncertainties are estimated to be ±1° for plume divergence [29].

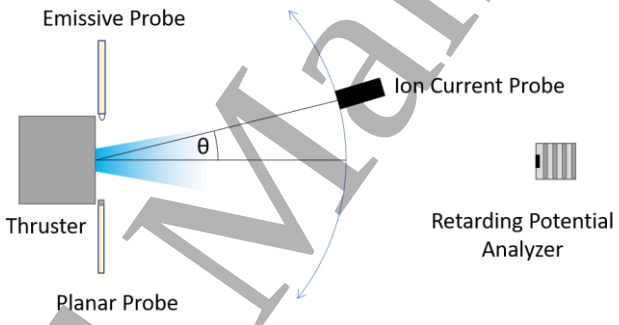

FIG. 4: Schematic of the experimental setup.

Ion energy distribution function (IEDF)

IEDF of ions accelerated form the thruster was measured by a retarding potential analyzer (RPA) placed 30cm downstream of the thruster exit along the thruster axis. The RPA operates by applying a positive voltage to a screening grid with respect to ground, which repels ions of energy/charge below the bias voltage and measures the remaining ions by a negative biased planar probe. By sweeping this bias voltage and differentiating the measured ion current with respect to the voltage, the ion energy

distribution is calculated. The RPA in this work utilized a 4-grid system, allowing greater precision in energy measurements, and has been used and described elsewhere [20,30].

2.3. Thrust and Thruster Performance

The thrust was measured using a torsion balance thrust stand (Fig. 5) with an estimated resolution of 0.02mN. The thruster is fixed on the arm with a commercial (Riverhawk 6032-800) flex pivot. During the thruster operation, the thrust force is applied to the arm causing the arm to displace with respect to the pivot. The resulting torque is resisted by the flex pivot and is directly proportional to the steady-state displacement of the thrust arm:

$$T = k_{eff}\left(x - x_{equil}\right), \tag{6}$$

where T is thrust, k_{eff} is the effective spring constant, x is the measured position and x_{equil} is the equilibrium position. The displacement is measured using a vacuum-compatible Micro-Epsilon optoNCDT 1420 laser sensor. During the thruster start-up, turn-off or significant thruster changes, the arm may oscillate. For damping of these oscillations, eddy-damping was implemented using a permanent magnet and an aluminum block attached to the arm. Tensions exerted by the thruster wiring and the flexible silicon gas line required direct measurements of the effective spring constant k_{eff}. This was achieved by measuring the arm displacement while electrostatic fins applied a known force, following a method described in Ref. [31]. The fin voltage-force response was measured using a precision balance over a range of fin separation distances. The thruster efficiency, η, was calculated using the measured thrust T, and the measured input parameters, including the mass flow rate $\dot{m}$, and input power P, as $\eta = T^2/2\,\dot{m}P$. The input power was calculated through the product of the measured traces of discharge current and anode voltage. Cathode power losses were not included.

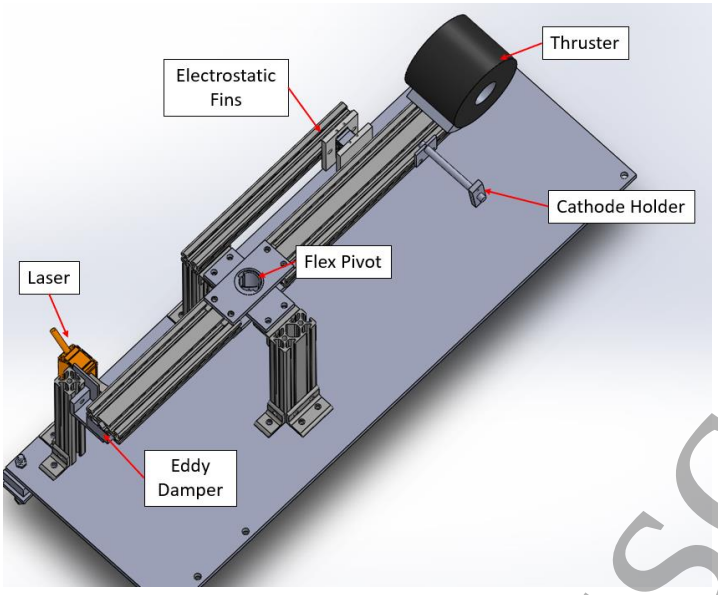

FIG. 5: A schematic of the thrust-stand used in the described experiments.

2.4. Measurement Procedures

For thrust measurements, the following procedure was used throughout all experiments described in this paper: the thruster was ignited and allowed to run for several minutes to allow the thrust stand to settle at the steady-state placement corresponding to the balance between the thrust force and the pivot restoring force. The arm displacement was then measured, and the thruster was turned off. The displacement with time was measured as the arm returned to equilibrium. A damped sine wave of the displacement oscillations was fitted to determine the equilibrium displacement at the time before the thrust was turned off [17]. Then, the total displacement due to thrust was calculated. After repeating this process at the same parameters for a total of 5 times, the thruster would be kept off and the electrostatic fin force-displacement would be measured to re-calculate the effective spring constant.

Time-dependent IEDF was determined by utilizing the entrainment of the oscillations with the anode voltage oscillations. This equalizing of frequencies allowed the RPA collector current signal to be separated by phase of the anode oscillation to deduce the time-dependent IEDF. This procedure is outlined in Ref. [32]. The same approach was repeated for the analysis of the ion current oscillations. It allowed the phase angle between these oscillations to be determined, which is one of the parameters in Eq. (1). The phase shift between oscillating signals was then calculated via the signal demodulation method.

Note that the plume probe displayed a low-pass filter effect due to some capacitance in the system, which both slightly smoothed out the data and added a time delay to the measured oscillating signal. This time lag was independently measured without thruster operation by running a sinusoidal current directly through the probe connected to the function generator to determine the phase shift-frequency relation. This quantity was later applied to offset the measured phases. Another quantity known to cause time lags was the transit time for the ions to reach the probe. This was accounted for by calculating the transit time from the known probe distance, L, and the measured ion velocity, V_i, as L/V_i.

2.5. Hybrid Code

In support of experimental efforts, we conducted an analysis of a modulating thruster with a 1-D fluid-kinetic hybrid code developed by G. Hagelaar [33–35]. These simulations provided insight into the processes in the thruster channel through which modulation affected thruster performance that were difficult to measure experimentally. This hybrid code treats ions and neutrals kinetically as particles through the use of super particles in the Particle-in-Cell simulations, while fluid equations describe the electrons. The code provides distribution of plasma properties in the axal direction along thruster channel and, partially, in the near field plasma plume. Specifically, the hybrid simulations were performed to answer the following questions: (i) Can a one-dimensional axial model capture the measured resonant behaviour of modulation? (ii) How the modulation affects ionization and acceleration regions in the thruster channel? (iii) Why does the measured phase behaviour exist (see Sec. 3.4)?

The hybrid model operates in the following method: at the beginning of each time step, the ion super particles are accelerated by the electric field in the system, after which the aggregate positions are used to calculate plasma density (due to quasineutrality). The electron temperature is then calculated through the electron fluid equation for energy balance, which allows the electric field to be calculated by the electron fluid momentum balance equation. This allows the process to repeat as the ions are stepped forward in time again. More information on the hybrid model can be found in References [34–37]. This model incorporates an anomalous energy loss term W to account for the electron energy that is typically lost to walls, the radial dimension, or field fluctuations, and is of the form:

$$W = \frac{3}{2}\nu_\varepsilon T_e e^{-\left(\frac{2U}{3T_e}\right)}, \tag{7}$$

where T_e is electron temperature, ν_e is anomalous energy loss frequency, and U is the reference electron energy. Both ν_e and U are treated as simulation parameters to be adjusted to fit the steady discharge case to experimental measurements. This model of anomalous energy losses is further described in Ref. [38].

A limitation of a one-dimensional model is that a CHT uses a two-dimensional magnetic field topology with a diverging magnetic field, especially in the cylindrical part of the channel (Fig. 2). Only the radial component of the magnetic field along the axis of the channel median was utilized for these simulations (Fig. 6), however it is acknowledged that in general simulating such a thruster requires three or, at least, two dimensions. Other input parameters such as thruster size, mass flow, and anode voltage were used from the experimental regime. The thruster channel was separated into two regions, the annular and cylindrical region, with differing wall losses, anomalous energy loss frequency, and Bohm parameter for each. The electron-wall collision frequency was set as 10 MHz in the annular region [33], 5 MHz in the cylinder region, and 0 MHz in the plume. The energy fitting parameter for anomalous losses U was set to 20eV as in previous simulations [39]. Measurements of the mobility, electron temperature, and plasma potential from previous works [21] provided targets for parameter scans of the Bohm coefficient and the anomalous energy loss frequency ν_ε. The resulting Bohm parameter was 3.0 in the annular region, 0.5 in the cylinder region, and 1.0 in the plume. The anomalous energy loss frequency ν_ε was 1.3 MHz in the annular region, 0.7 MHz in the cylinder region, and 0.7 MHz in the plume.

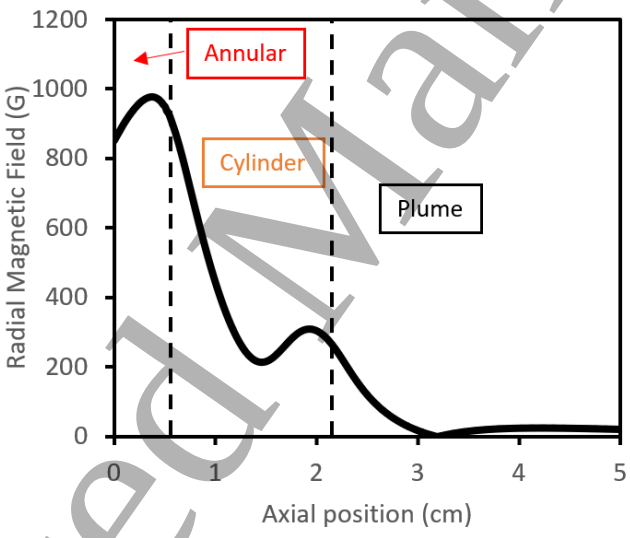

FIG. 6: Radial magnetic field of the CHT along the channel median used in hybrid simulations. Annular, cylindrical, and plume regions are shown for reference. Anode is located at the 0cm axial position while 5cm is the simulation end.

3. Results and Discussion

3.1. Current Response

The 2.6cm CHTpm2 was modulated at a discharge voltage of 220V with a sinusoidal oscillation of 40V amplitude and varying frequency. The unmodulated discharge current and on-axis plume ion current density is shown in Fig. 7, where the natural frequency of 10 kHz on both the ion current and discharge current is visible in Fig. 7b. Illustrative current and energy responses measured in the plume at two frequencies of 9 and 11 kHz are shown in Fig. 8. Similar to previous experiments with electromagnetic CHT [9], this permanent magnet CHT exibits a resonant behaviour too. Specifically, it was found that at the natural breathing frequency of 10 kHz, the amplitude of the current oscillations reached a maximum which was approximately equal to the mean current value (Fig. 9a). Measurements of the total ion current and the discharge current revealed a dependency on the modulation frequency, which increased with frequency with a maxima near resonance, but remained higher above resonance than below (Fig. 9b). This corresponds to an increase in the propellant utilization from 102% at no modulation to 107% at the maxima with associated error of ±2% from the ion current measurements and mass flow uncertaitny. This high propellant utilization can be attributed to a significant population of multi-charge ions that is typical for CHTs [29]. Note that discharge current rose proportionally to the ion current and current efficiency remained roughly the same at 50%.

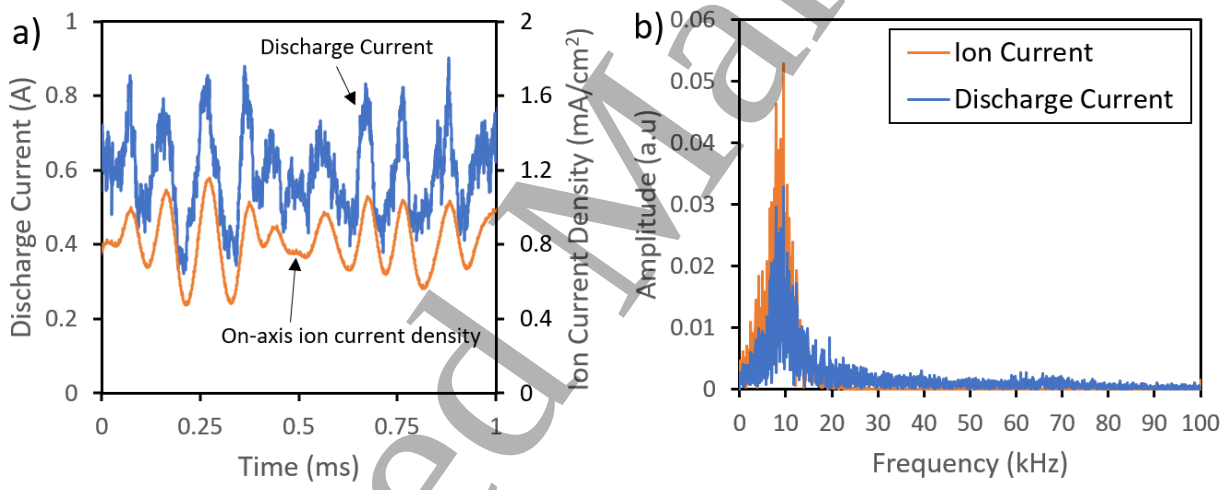

FIG. 7: Measured discharge current and on-axis ion current density for the unmodulated CHT operating at the discharge voltage of 220V and 4 sccm mass flow: a) time-trace of the currents, b) FFT of the currents.

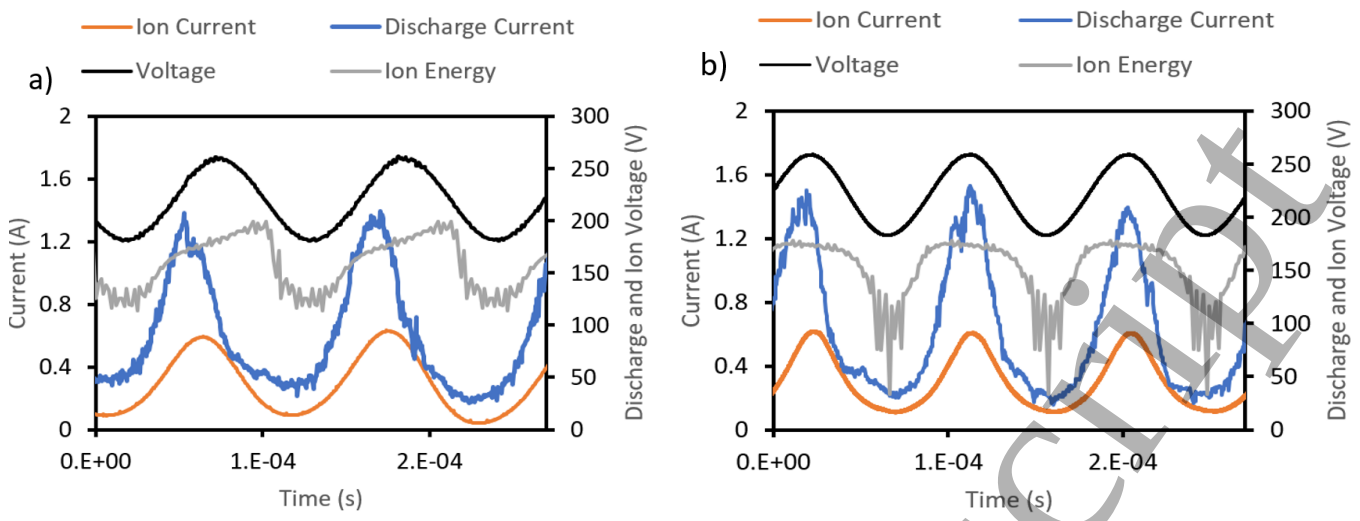

FIG. 8: Measured discharge voltage, discharge current, ion energy/charge, and ion current vs time for the CHTpm2 operating at the discharge voltage of 220V with voltage modulations of ±40V and mass flow of 4 sccm: a) modulation frequency is 9kHz, b) modulation frequency is 11kHz

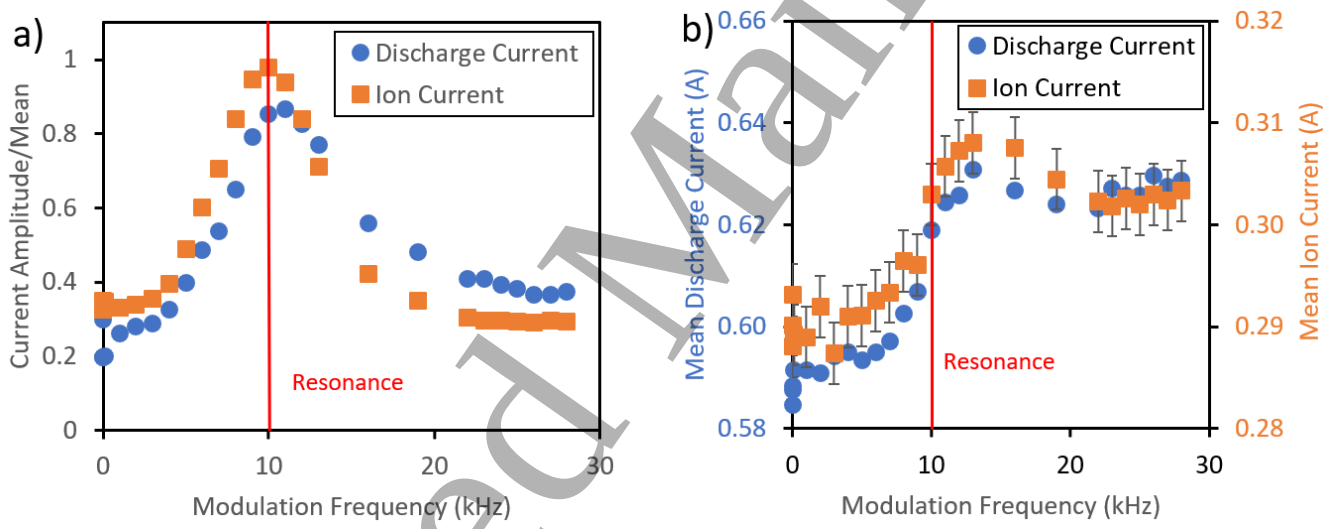

FIG. 9: Measured discharge current and ion current mean and amplitude as the function of the modulation frequency for ± 40V modulation amplitude: (a) Normalized amplitudes of the discharge and ion currents; (b)Time-average discharge current and ion current. The red line corresponds to the natural breathing frequency.

The increase of the ion current at higher frequencies can be explained by the observed changes in the phase difference between oscillations of ion velocity and ion density. It was predicted in Ref. [9] that modulating the thruster in resonance with the natural breathing frequency would cause an increase in the ion current due to the ion density and ion velocity oscillations coming closer into phase. Our measurements of the phase between plasma density at the channel exit and ion energy in the plume (accounting for the ion transit time from channel exit position) show that as modulation approaches the resonance condition the phase lowers

to a value of 60° (Fig. 10) and then, reduces even further at frequencies above resonance. This behaviour of the phase difference explains the increase of the ion current to its maximum value of 0.31 A at the resonant frequency which does not drop significantly at higher frequencies (Fig. 9b).

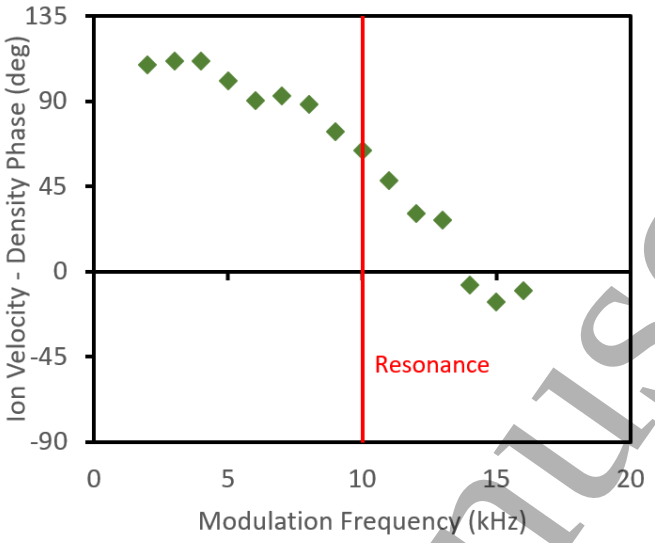

FIG. 10: The change in phase angle between ion velocity and ion density as a function of the modulation frequency. Standard error in ion velocity-density phase measurements is ±3°. The red line corresponds to the natural breathing frequency.

Measurements of the discharge and ion current phase ϕ_d and ϕ_i found alignment of the ion current and measured ion energy at resonance, while discharge current and discharge voltage aligned at slightly above resonance at ~13 kHz (Fig. 11). As observed in Eqs. 1 & 2, both discharge power and thrust are maximized when the discharge and ion phase are zero. Thus, to maximize the increase of the thruster efficiency, oscillations of the discharge current and the discharge voltage need to be out of phase to minimize the input power, while oscillations of the ion current and the ion energy need to be in phase to maximize the thrust power. Results shown in Fig. 11 provides some possibility for such performance improvement to be realized. Specifically, there appears to be desirable trends in differences between ion (current and energy) and discharge (current and voltage) phases (Fig. 11). Errors on the phase measurement are about ±3° for ion phase at frequencies near resonance and increase to ±25° off-resonance, while discharge phase error is much lower at ±1° near resonance and ±2° off-resonance. Phase error is discussed in Appendix B.

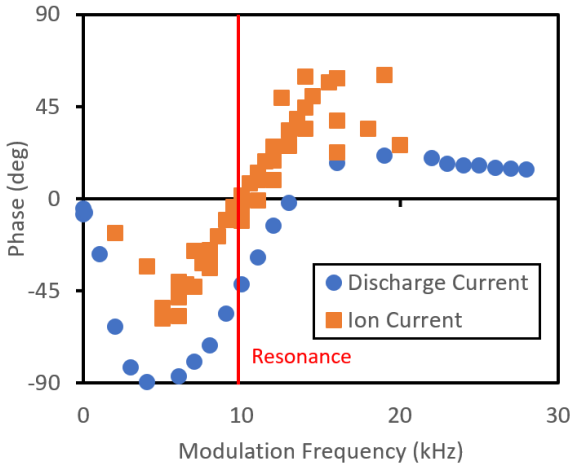

FIG. 11: Measured discharge current-discharge voltage and ion current-ion energy phase angles with respect to modulation frequency for a modulated CHT. The red line corresponds to the natural breathing frequency.

3.2. Ion Energy and Voltage Drop

Time-resolving RPA measurements in the plasma plume showed that IEDF oscillations follow the externally driven anode voltage modulation. This is in agreement with previous measurements of the IEDF from CHTs using time-resolving laser-induced fluorescence diagnostics [40]. Unlike the anode voltage oscillations, the shape of the IEDF oscillations is not always sinusoidal, appears to depend on the modulation frequency. This non-sinusoidal shape is also observed in the discharge current (Fig. 8). RPA measurements revealed an increase in the time-averaged ion energy as voltage modulation frequency approaches the frequency of the resonant frequency (frequency of natural breathing oscillations) (Fig. 12). This is due to the reduction of the phase difference between the ion energy and the ion current oscillations (Fig. 11).

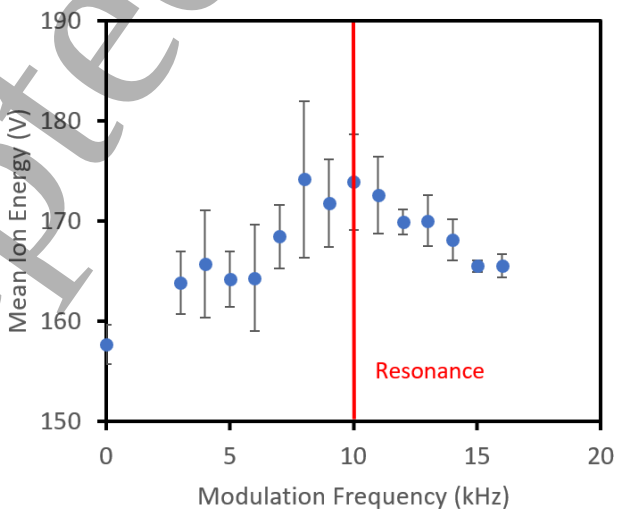

FIG. 12: The effect of modulation frequency on the time-average ion energy of a modulated CHT with voltage 220V and modulation amplitude ±40V. The red line corresponds to the natural breathing frequency.

It is important to note that the amplitude of the ion energy oscillations decreases from 40V at low modulation frequencies (3 – 6 kHz) to 20V at modulation frequencies near the resonance (10kHz) and at higher frequencies (Fig. 13a). A reduction of the ion energy amplitude should limit the increase of thrust (Eq. (1)). A smaller ion energy amplitude $\hat{V}_i$ lowers the thrust by the second term on the right-hand side of Eq. (1).

It is also interesting to look at the possible correlation between IEDF oscillations and oscillations of the plasma potential at the channel exit, which is indicative of changes of the profile of the voltage potential drop between the anode and the cathode. This voltage potential drop includes the ionization and the ion acceleration regions of the thruster. The measured plasma potential at the channel exit was found to have little change in time-average value, and consequently the time-average value of the anode to channel-exit voltage drop was relatively constant at 180V. However, the time-dependent changes of the voltage drop with the modulation frequency behave differently than the time-averaged voltage drop. There were significant oscillations in the voltage drop that appeared to vary with the modulation frequency. The amplitude of these oscillations appeared to lower at high frequencies (Fig. 13b), much like the ion energy (Fig. 13a). If the voltage drop inside the channel only oscillates with ±20V of the applied ±40V amplitude, the remainder must be in ±20V amplitude potential oscillations in the plasma plume.

It is notable that the mean ion energy never exceeded the maximum energy (180 eV) which a singly charged ion could acquire by a monotonic acceleration in the voltage drop value of 180V. The ion energy amplitude approximately tracked the channel voltage drop amplitude (Fig. 13). As such, it is hypothesized that the oscillations of plasma potential outside of the thruster has little effect on the ion acceleration. This may be due to the large axial components of the magnetic fields in the CHT causing the electric fields to have large radial components. Accordingly, the potential drop outside the channel would result in radial ion acceleration, which the axially-located RPA would not measure, nor would thrust increase. Consequently, any movement of the acceleration region out of the thruster would result in limitations on thrust in two ways: lowered ion energy oscillations and increased plume divergence.

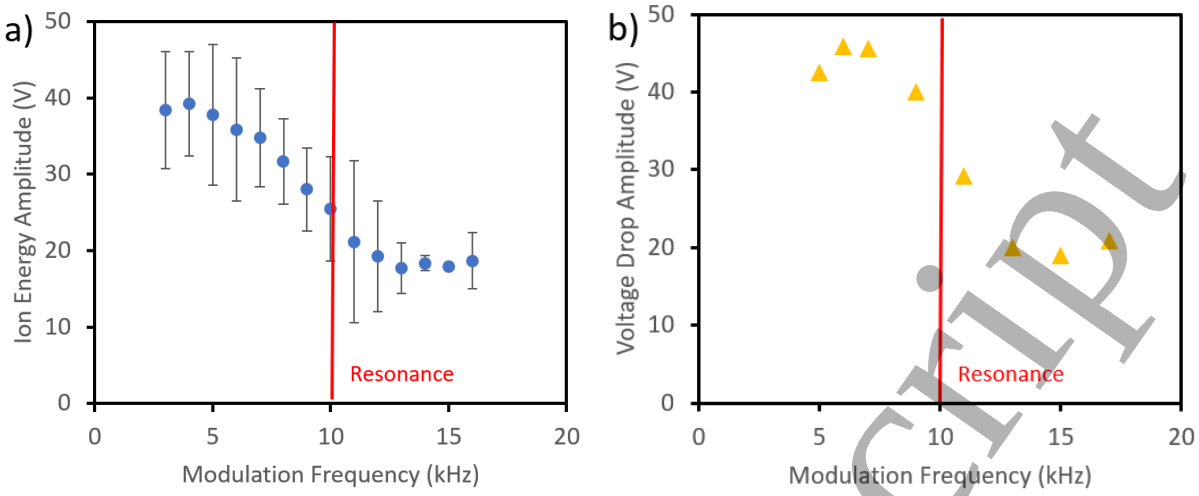

FIG. 13: (a) The decrease in the ion energy amplitude with modulation frequency and (b) the decrease in the thruster channel voltage drop amplitude with modulation frequency. The red line corresponds to the natural breathing frequency.

3.3. Performance

Thrust was measured for the CHTpm2 thruster operating with several modulation frequencies (0, 7, 9, 11, 16 kHz). For all these modulations, the amplitude was 40V. This was the maximum achievable amplitude of modulations at which the thruster operated without self-extinguishing the discharge. Fig. 14a shows that the thrust reaches its maximum value at the resonant frequency of 10kHz. The measured thrust increase is 4%. This result is qualitatively in agreement with predictions of Ref. 9 which attributes the thrust increase to an increase of the fraction of high energy ions when oscillations of the ion current and the ion energy are in phase. For this *in phase* case, the maximum theoretical increase of the thrust can be calculated using Eq. (1). Using the measured amplitude of the ion energy oscillations (AC component), 40 eV, and the mean energy, 160 eV (Fig. 12 & 13), the theoretical thrust increase is 6%. This is more than 30% larger than the measured maximum increase of the thrust at the resonance frequency (Fig. 14a). Note that errors in thrust measurements here were found by the standard error of all measurements at each regime and while this was on average ±0.05mN, the error at 11 kHz was quite high and comprised about 50% of the measured increase. While slightly lower in thrust improvement, the 9 kHz modulation frequency regime showed similar gains with very small deviations between measurements, which implies there is a definite thrust increase. Despite the measured thrust increase, voltage modulations at the resonance frequency appeared to have an insignificant effect on the thruster efficiency (Fig. 14b). This is because the input power also increases at the resonance frequency, and any increases that were observed were within the high uncertainty of efficiency measurements at ±3%. This high uncertainty was in large part due to the mass flow error of ±0.1 sccm.

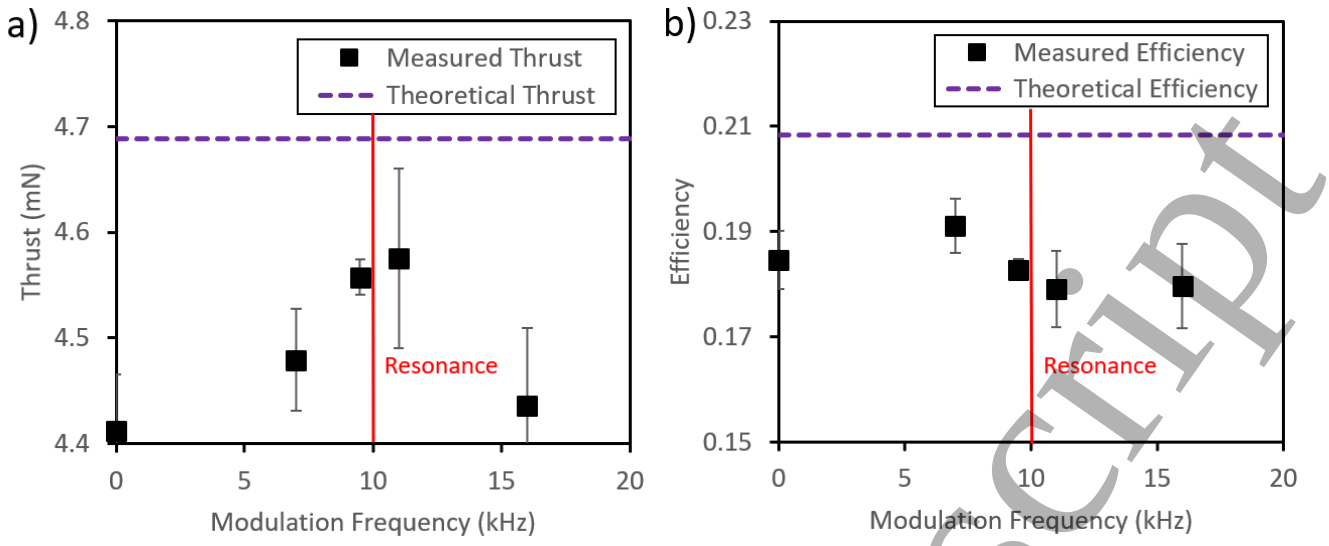

FIG. 14: Measured thrust (a) and efficiency (b) at varying modulation frequency for a CHTpm at 220V and 4sccm with modulation amplitude 40V. The calculated ideal modulated thrust and efficiency by Eq. (1) is shown for comparison. Error bars of thrust correspond to standard deviation over multiple measurements, and error for efficiency includes mass flow uncertainty averaging ±3%. The red line corresponds to the natural breathing frequency.

3.4. Plume Divergence

The dependence of the plume angle on the modulation frequency was found to be non-monotonic (Fig. 15). The plume angle tends to be generally larger with modulations. The maximum increase of the plume angle (about 5%) with respect to the non-modulating thruster case occurs near the resonant frequency of the modulation. Error here is estimated to be roughly ±1° as with previous measurements with this diagnostic [29]. While this error is considerable compared to the changes in plume angle, there is a clear trend with frequency with a maximum at resonance. Despite relatively small changes in the absolute plume angle, the increase of the plume divergence could cause the reduction of the thrust due to defocusing of the ion flow. The maximum reduction estimated as the cosine ratio of the plume angle (60.8° for no modulation and 63.7° for modulating near resonance) could reach 10%. This thrust reduction due to the increased plume divergence could account for the lower thrust value measured with the modulation as compared to that predicted by Eq. (1). This increase in the plume divergence is consistent with the outward shift of the acceleration region during strong breathing oscillations experimentally observed in other works for annular Hall thrusters [41].

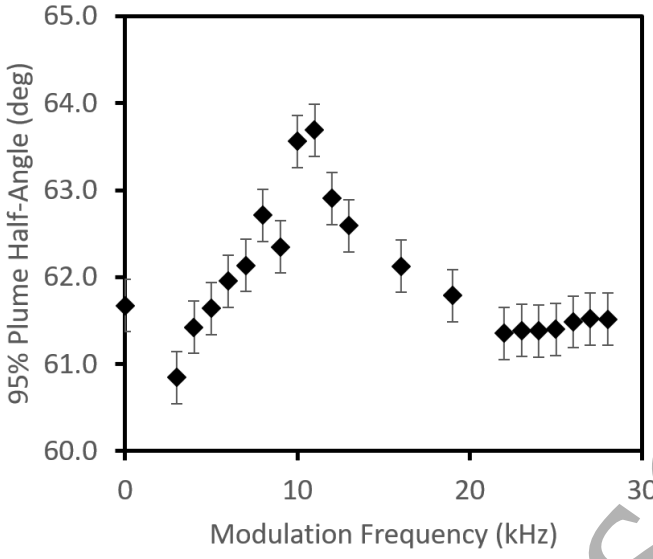

FIG. 15: The effect of modulation frequency on the half-plume angle of a CHTpm2 operating with 220V with modulation amplitude ±40V. The uncertainties in the plume angle measurements are ±0.3°

4. Modelling

With limited diagnostic capabilities inside the thruster channel, simulations of the CHT were conducted to determine the mechanisms by which ion energy changed and the acceleration region moved. Understanding why the discharge and ion phase-frequency relationship exists is of interest, as it may potentially help to find ways for performance improvements for modulated thrusters

4.1. Simulation and Experiment

In general, 1D hybrid simulations of the CHT resulted in similar behaviour as what was measured experimentally – propellant utilization, current utilization, and voltage utilization were among similar levels, as well as the plasma parameter-frequency behaviour already discussed. One key difference was a natural breathing frequency of the oscillations, which in simulations was found to be 23kHz, compared to the 10kHz of the experiments. Attempts to achieve the same frequency during parameter scans of the simulations were not successful, which may be due to several factors such as the one-dimensional approximation of the simulations and poor knowledge of the anomalous mobility. The one-dimensional approximation, as is used in this model, can be especially critical for cylindrical thrusters with strong two-dimensional effects. The value and profile of the anomalous mobility remains one of the least known factors, despite its strong influence on the breathing mode parameters such as frequency and amplitude. Yet, another significant factor not captured by the simulations are the temporal variations of the parameters, such as electron mobility, which has been demonstrated by recent experimental measurements [42]. Despite all these limitations

of the theoretical model, the modelling reproduces the main features of the experimental results, as can be seen in the appendix in Fig.'s A.1-3.

4.2. Acceleration Region Movement

The acceleration region is defined as the region in which ions are accelerated due to a high electric field. For annular Hall thrusters, the ion acceleration region is typically located in the region of high magnetic field where the electron cross-field mobility is substantially reduced. For the CHT, the situation is different as the magnetic field is highest near the anode and decreases axially towards the exit. Experiments demonstrated that the cross-field mobility is smaller in the cylindrical portion of the thruster away from the anode [43]. As such, the electric field profile in the CHT has no well-defined maximum and the acceleration region must be defined another way. For the sake of this analysis aimed to qualitatively explain experimental results, the acceleration region was defined as the axial position at which ions are accelerated to 110eV (half the applied voltage). This energy level was partly chosen for graphical convenience, as the associated acceleration region position is near the channel exit, and it is important to note it does not represent any boundary of the acceleration region but rather an indicator of the position. The time-average position of the acceleration region (Fig. 16) appears to move outward to the thruster channel exit near resonant frequencies (23 kHz), which is consistent with the measured increase of the plume divergence shown in Fig. 15. Other definitions of the acceleration region position, such as defining it by a fixed low plasma, showed similar outward movement near resonant frequencies.

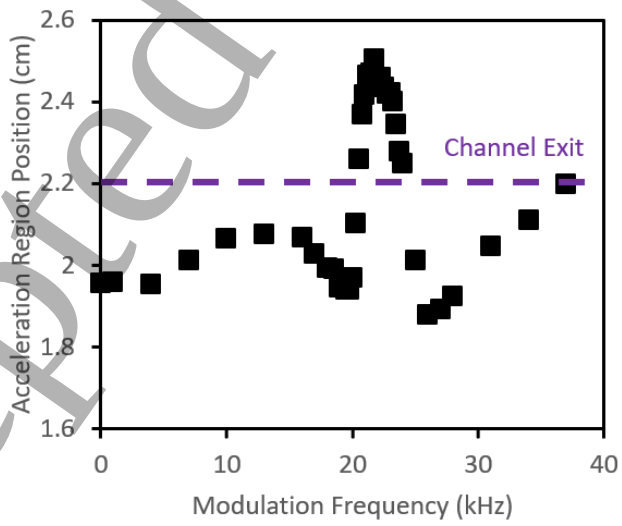

FIG. 16: Outward movement of the acceleration region near resonant modulation frequency for a simulated Hall thruster with modulation amplitude ±40V. Channel exit shown as a dashed line for comparison.

4.3. Ionization Region

It is commonly accepted that in Hall thrusters, the ionization of the propellant gas occurs along the whole channel, but there is a region of most intense ionization – the ionization region – where ion density grows rapidly while the neutral density is consumed. For the sake of our analysis of simulation results and their qualitative comparison with experiments, the placement of the ionization region in the thruster channel was defined by the axial position at which the neutral density was depleted by some predefined value. Neutral density exponentially decreases with axial position, often with no defined beginning nor end. This necessitates some definition of the region which can be applied consistently across all simulations, and so the bounds of the region were defined by when the density had lowered by a portion of the total density. More specifically, the beginning of the ionization region was defined as the position at which neutral density fell 5%, while the end of the ionization region was defined as the position at which it lowered by 95% of the value at the anode. A comparison across frequencies reveals that for voltage modulation with a resonant frequency, there is significant spatial compression of the ionization region (Fig. 17) which is also shifted closer to the anode. Fig. 17 displays the spatial position of the beginning and the end of the ionization region with respect to the anode placement.

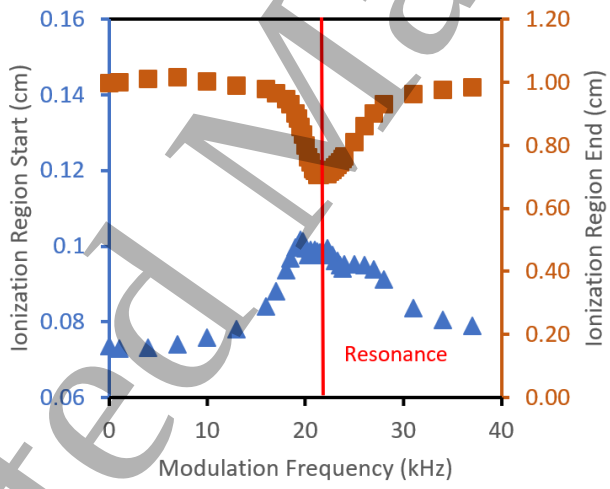

FIG. 17: Compression of the ionization region for a simulated Hall thruster when modulating near resonant frequencies. The red line corresponds to the natural breathing frequency.

This compression of the ionization region is driven by the enhanced ionization rate due to the increase of the electron temperature in this region. A time-average value of the electron temperature in the middle of the ionization region increased by 1eV at resonance from the natural value of the non-modulated thruster (Fig. 18). Furthermore, the amplitude of the electron temperature oscillations was amplified at these resonant frequencies, allowing the peak electron temperature to increase ~4.5 eV beyond the time-average value of the unmodulated case (Fig. 18). This higher electron temperature corresponds to double

the ionization rate compared to the unmodulated case. For future studies, it will be important to experimentally validate this predicted increase of the electron temperature.

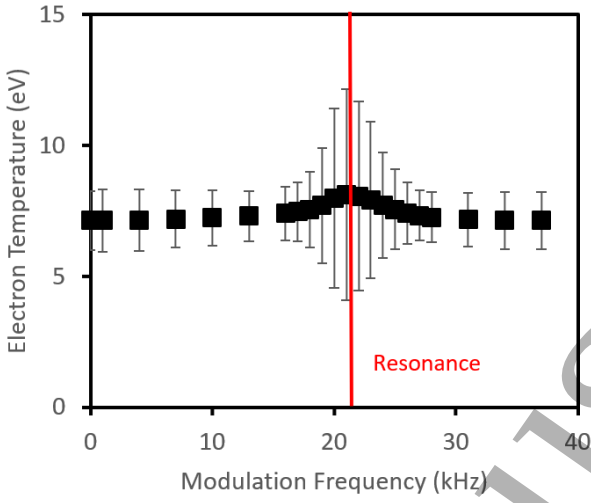

FIG. 18: Increase of electron temperature for a simulated Hall thruster when modulating near resonant frequencies. Electron temperature is taken in the middle of the ionization region with error bars representing amplitude of temperature oscillations. The red line corresponds to the natural breathing frequency.

Note that the simulations in this work did not include multiple charged ionizations, and so the propellant utilization did not exceed 100%, nor was there an increase in the ion current as was observed in the experiments. In simulations, the ionization was observed as a moving ionization front, which periodically travelled towards the anode as it increased in ionization before disappearing near the anode where the electron temperature was too low to sustain an intense ionization. The dynamics of the ionization front and associated motion of the ionization region bear investigation as it is primarily responsible for the phase-frequency relationship are shown in Fig. 11.

4.4. Control of phase between discharge voltage and current

Phasing between the current and the voltage is one of the primary factors in whether thrust increases/decreases, and whether input power increases/decreases: when the discharge phase (discharge current vs discharge voltage) or ion phase (ion current vs ion energy related) become zero, the discharge power or thrust respectively increase. Experimental measurements (Fig. 19a) and simulation results (Fig. 19b) of the discharge and ion phase show a clear dependency of these phases on the applied modulation frequency. In both experiments and simulations, the ion phase falls to zero near resonance, while the discharge phase becomes zero at a slightly higher frequency. It is also notable that near resonance the phase-frequency relationship appears

linear (Fig. 19). Simulations of the total ionization (ion source term integrated over the simulation length) occurring in the thruster can explain this linear relationship between modulation frequency and discharge phase as well as the shape of the current oscillations. This ion source term is closely related to the ion current, and consequently the discharge current, due to the relative timescale of ionization ($\sim 10^{-4}$ s) and electron residence time ($\sim 10^{-7}$ s), as newly created electrons stream to the anode and contribute directly to the discharge current. The total ionization is related to the ion current by the current continuity equation:

$$eA\int_0^L S_{ion}\partial x = I_i + \int_0^L \frac{\partial n_e}{\partial t}\partial x, \tag{8}$$

Where A is the channel area, L is the simulation length, and S_{ion} is the ion source term, which is the product of neutral density n_n, plasma density n_e, and the ionization rate coefficient K. The ionization rate coefficient is the integral of the electron-impact ionization cross section over a Maxwellian velocity distribution $f(v)$:

$$S_{ion} = n_n n_e K, \tag{9}$$

$$K = \langle v\sigma \rangle = \int_0^\infty v f(v)\sigma(v) dv, \tag{10}$$

The ion current oscillations are governed by the oscillations of all parameters in Eq. (9). As an example, oscillations of the neutral density, plasma density, and ionization rate coefficient in the middle of the ionization region, as well as the total ionization (source term integrated over channel) are shown in Fig. 20, where all parameters have been normalized by their time-average value. The sharp-tip shape of the total ionization, and consequently the current, is initiated by the rise of the ionization rate caused by an increase of the electron temperature, which results in the rapid increase of the plasma density by ionization of neutral atoms. This continues until the neutral density is depleted, at which point the ionization sharply drops until neutral density and electron temperature raise again for the cycle to continue.

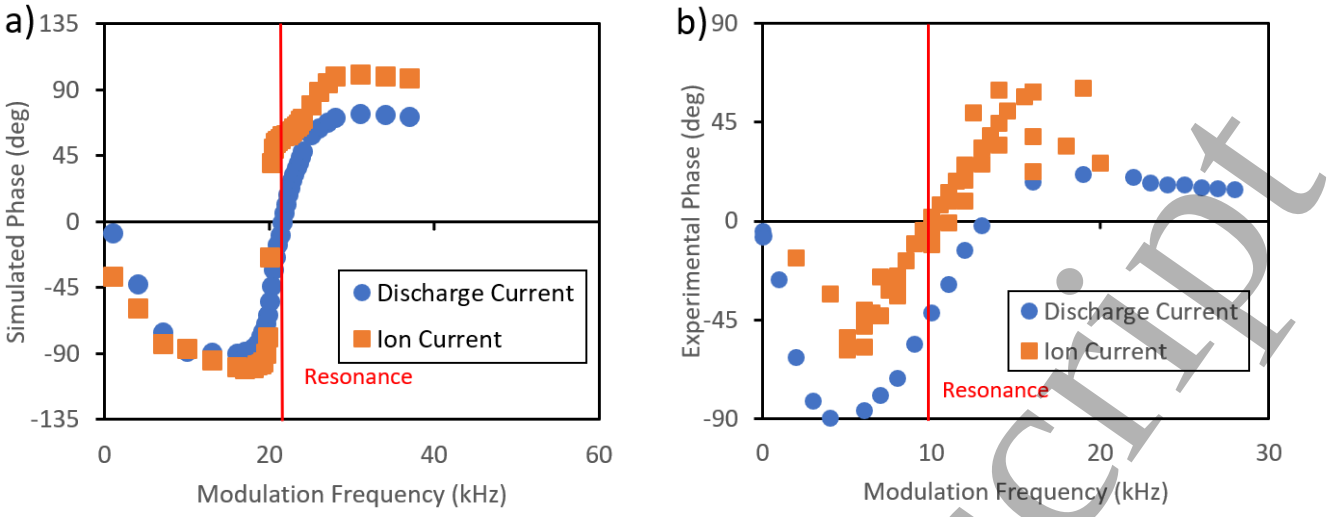

FIG. 19: Phase difference between anode voltage oscillations and current oscillations with respect to modulation frequency from (a) numerical simulations of a CHT and (b) experimental measurements of a CHT with voltage 220V and modulation amplitude ±40V. The red line corresponds to the natural breathing frequency.

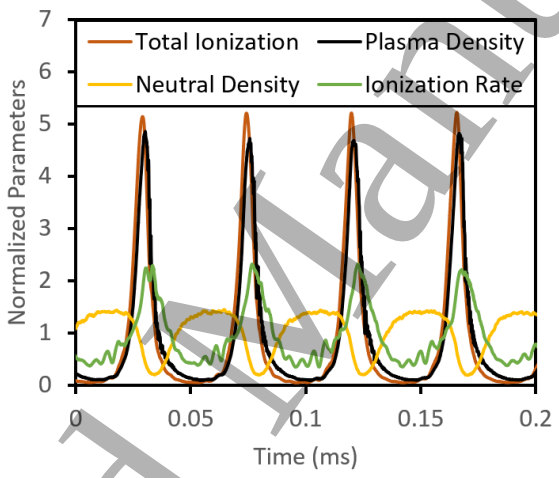

FIG. 20: Ionization source, plasma density, neutral density, and ionization rate coefficient in the ionization region normalized to their time-average mean vs time for a simulated CHT with modulation frequency 22 kHz and amplitude ±40V.

Time traces of anode voltage and the total ionization for several modulation frequencies reveals a consistency in the shape of these oscillations, but differences in the relative phase between the ionization and voltage oscillations (Fig. 21). The rise-time of ionization (τ_{ionize}) appears to be consistent across modulation frequencies, with the initial rise corresponding roughly to the minima of the anode voltage. This basic picture provides some insight into the phase-frequency relationship – if anode voltage oscillates too slowly, ionization begins and depletes the neutrals before the voltage reaches its maximum (negative discharge phase). If anode voltage oscillates too quickly, it may reach the maximum before ionization reaches its own maximum (positive

discharge phase). For the generation of the maximum ion power flux, the ionization should be at its maximum when the voltage is at the maximum as that will increase the energy of the ions in the thruster.

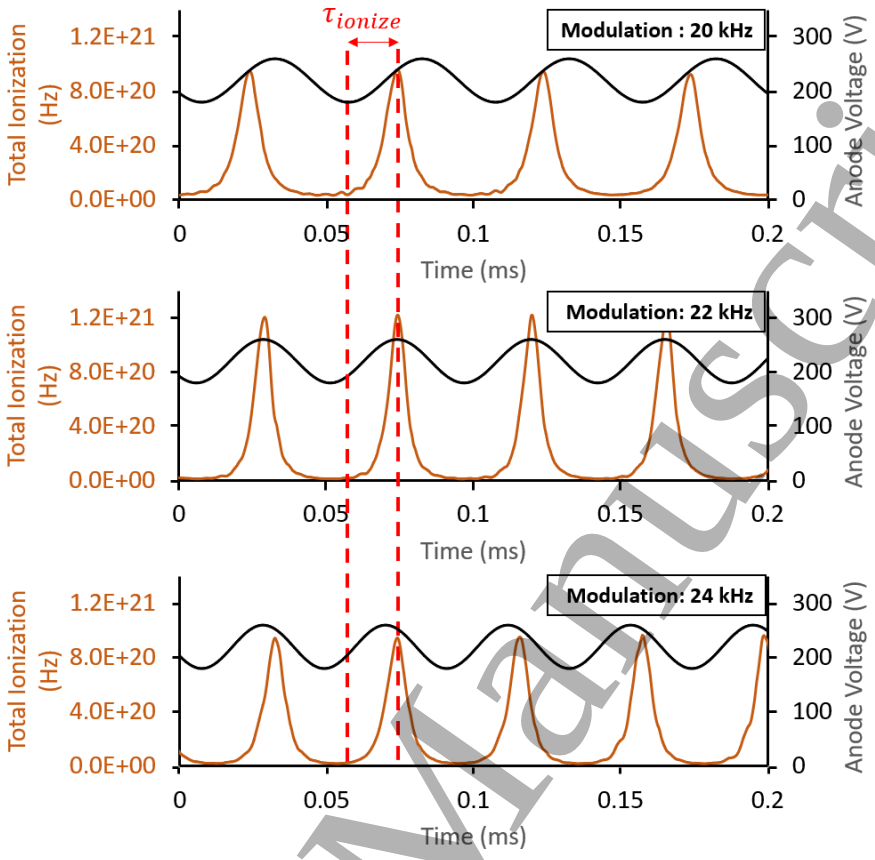

FIG. 21: The oscillations of the total ionization in a simulated Hall thruster for three modulation frequencies (20, 22, and 24 kHz) with modulation amplitude ±40V. Associated rise-time of ionization is shown which appears constant with frequency.

The linear phase-modulation frequency relationship can be found to be due to this relatively constant ionization rise-time. Due to the aforementioned timescales and relationship between current and total ionization Eq. (8), the phase between the anode maxima and the ionization source maxima corresponds to the discharge phase $\theta_{discharge}$ (Fig. 22). The discharge phase can then be written as the sum of the phase at which the ionization begins to rise $\theta_{threshold}$ and the phase over the rise-time of the ionization τ_{ionize}:

$$\theta_{discharge} = \theta_{threshold} + 2\pi f_{mod}\tau_{ionize} \tag{11}$$

Assuming the threshold phase and rise-time remain constant over modulation frequency, the phase should remain linear to the modulation frequency, which appears to be the case for frequencies close to resonance (Fig. 19). The average threshold phase

at which the ionization front forms can then be found through the y-intercept of the measured and simulated phase-frequency data in Figs. 19. The experimental discharge phase data provided a threshold voltage of 184 ±1 V (phase of -152° ± 6°). The same method applied to the simulation results provided a threshold voltage of 180 ± 4V (phase of -189° ± 19°). These show the ionization wave forms after the anode voltage reaches a minimum.

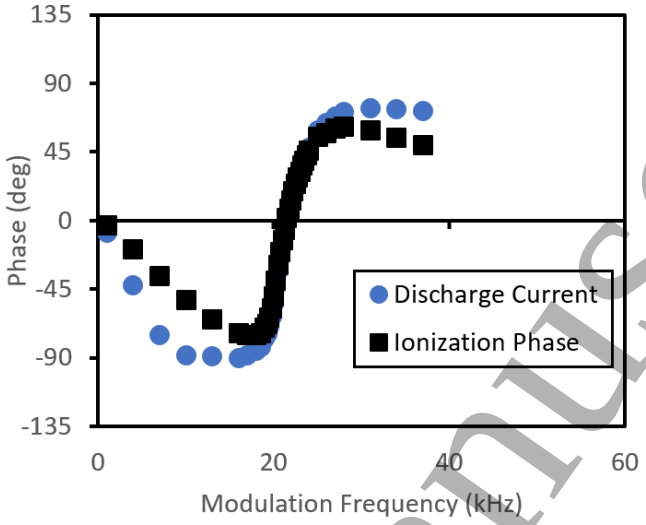

FIG. 22: Comparison between the discharge current-anode voltage phase and total ionization-anode voltage phase vs modulation frequency for a simulated CHT

The consistency of the rise-time and the threshold phase are of interest at these frequencies and bear some additional analysis. The threshold phase close to the minimum of the anode voltage is likely due to the combination of two factors: 1) the replenishment of neutrals at this phase and 2) the rise in electron temperature, which oscillates in phase with anode voltage, from its minimum. It is important to note the contribution of the electron temperature – Fig. 20 shows that neutral density replenishes well before the ionization picks up again, which corresponds to the electron temperature increase. The ionization rise-time was calculated by determining the average time between a 5% increase in the ionization source and a 95% increase and has been plotted against modulation frequency (Fig. 23). There it is observed that this formation time is initially about half the time at resonance compared to the natural. As modulation frequencies approach resonance, the rise-time appears to decrease to a minimum. Here, the timescale remains relatively constant over the frequencies close to the modulation frequencies while the phase-frequency dependence is linear. This minimum in ionization time appears to be due to the increased electron temperature and plasma density associated with the ionization region compression (Figs. 17 & 18).

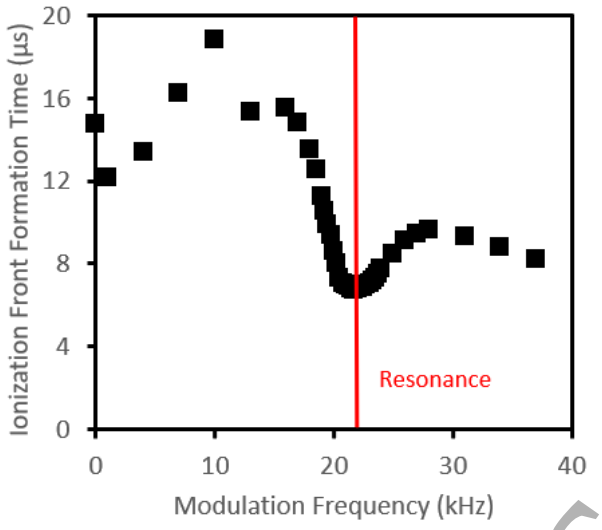

FIG. 23: The effect of modulation frequency on the ionization front rise-time (time to formation), with associated minima at resonant frequency. The red line corresponds to the natural breathing frequency.

5. Conclusions

Modulation of Hall thrusters represents an alternative method to alter thruster performance through electrical and ion phase engineering. From a practical standpoint, modulation is an attractive method to vary the thrust of a Hall thruster because it can potentially simplify the conventional design of the spacecraft Power Processing Unit (PPU). Due to the need to step up a low DC voltage from solar panels to several hundred volts for the thruster, voltage oscillations are already induced by the DC Boost Converter, which are then smoothed out by a capacitor. If modulating is effective in increasing performance, this would require minimal changes in the PPU to implement. With a simple alteration of existing power supplies, it can potentially be applied to any Hall thruster. By careful alignment of the phases of ion current and ion energy oscillations, thrust can be improved greatly compared to the same nominal discharge voltage with no oscillations. Great care must be taken, however, to understand how the discharge current oscillates, or any gains in thrust may be counteracted through gains in discharge power. Experimental measurements of the phasing revealed a slight difference between the ion current and discharge current oscillations of about 30-40°, indicating some capability to control their phasing in CHTs. The phase of ion energy-ion current was also found to align near resonance, spurring the increase of thrust.

While the CHT displayed some increase in thrust while modulating, it did not reach the ideal increase as calculated by Eq. (1). The measured improvement did match that predicted by Eq. (1) when inserting the measured plasma parameters, including plume divergence (Fig. 24). The primary reasons that the measured thrust was lower than this fundamental maximum modulated thrust were found to be due to increased plume divergence and lower ion energy amplitude. Further increases in performance

necessitate decreasing the plume divergence and increasing the phasing between ion current and discharge current. The dependency of ion and discharge phase on modulation frequency provides some capability for throttling thrust and power in the CHT. In addition, it would be interesting to explore the practical feasibility of predicted performance improvements with higher amplitudes of voltage modulation. In this respect, we encountered some difficulty in maintaining the CHT discharge when plasma density amplitudes get too high as the thruster may self-extinguish. Methods to maintain the discharge to enable such high-amplitude oscillations may be necessary for high-performance operation in such regimes.

The net thrust and discharge efficiency are the results of the spatial amplitude profiles and phase alignments of various plasma parameters. Our experimental results and simulations show complex spatio-temporal behaviour of the ion current, ion velocity and density during the breathing mode cycle. Efforts towards understanding the time-dependent anomalous mobility are critical towards developing simulations that can accurate capture these modulated thrusters, as they remain the largest uncertainty in simulations. The coupling of the ionization and acceleration region remains an obstacle towards the effort of controlling the plasma and performance, and so the application of the modulation concept on thrusters with high separation of acceleration and ionization regions, such as multistage Hall thrusters, may lead to higher performance.

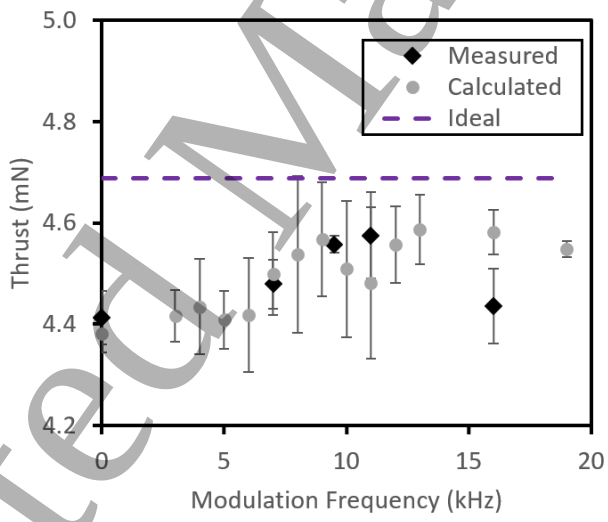

FIG. 24: Calculated, measured, and ideal thrust over modulation frequency for a CHT with mass flow 4sccm, anode voltage 220V and modulation amplitude ±40V.

Acknowledgements

The experimental work conducted at PPPL was supported by AFOSR grant FA9550-17-1-0010 and the US Department of Energy under contract DE-AC02-09CH11466. The authors would like to acknowledge Ivan Romadanov, Igor Kaganovich, and Tasman Powis for fruitful discussions as well as Gerjan Hagelaar for providing the hybrid simulation code.

Appendix A. Hybrid Simulations

One-dimensional hybrid simulations obtained similar results to the experimental regime despite the differences in magnetic profile. These similarities are largely qualtiative: comparative trends can be found though the values are different. Sample plots shown here include the discharge and ion current oscillation response to the input modulation frequency, which has a clear peak at the natural frequency of the system (Fig. A.1). Note that the amplitude $\hat{I}$ is defined here as:

$$\hat{I} = \sqrt{2}\, RMS(I(t) - \bar{I}) \tag{A.1}$$

Where $\bar{I}$ is the mean current. This formulation is equal to the peak-peak value for an offset sinusoid, however may give higher values for waveforms that are not sinusoidal, as is the case in the simulated discharge and ion currents (Fig. A.1). The simulated thrust was higher than the experiments (Fi.g A.2), however they both appeared to increase by about 5% near resonance. Curiously the maximum thrust for both appeared to be slightly above resonance, however there were few thrust measurements experimentally more measurements are required to make any conclusions. Like thrust, efficiency was higher in the simulations, but showed the same increase at low frequencies then decrease towards resonance as measured experimentally (Fig. A.3).

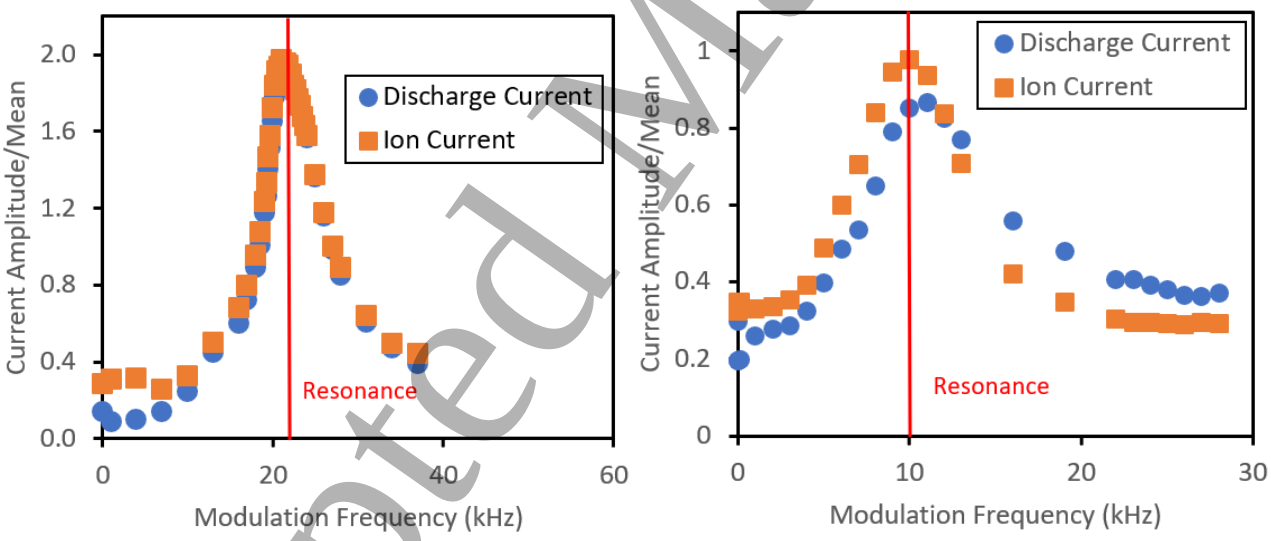

FIG A.1: Comparison of current oscillation amplitude vs the modulation frequency for a Cylindrical Hall thruster with input voltage 220V and modulation amplitude ±40V: simulations (left) and experiments (right). Amplitudes are normalized by the time-average value of the current. The red line corresponds to the natural breathing frequency.

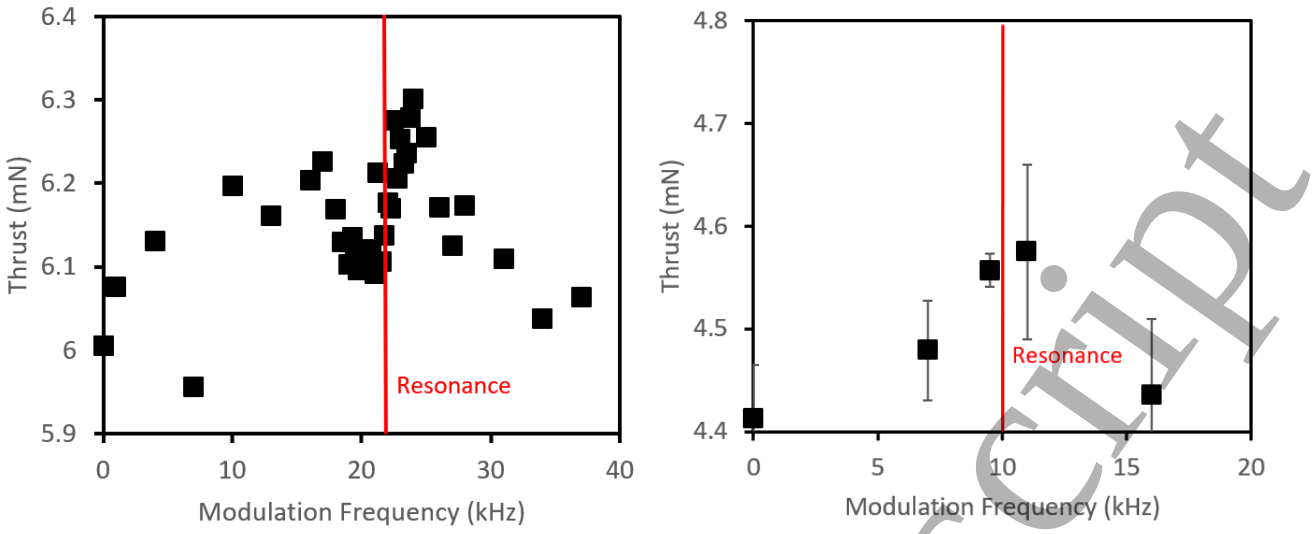

FIG A.2: Comparison of thrust vs the modulation frequency for a Cylindrical Hall thruster with input voltage 220V and modulation amplitude ±40V for simulations (left) and experiments (right). Error bars of experimental efficiency thrust correspond to standard deviation over multiple measurements as well as mass flow uncertainty averaging ±3%. The red line corresponds to the natural breathing frequency.

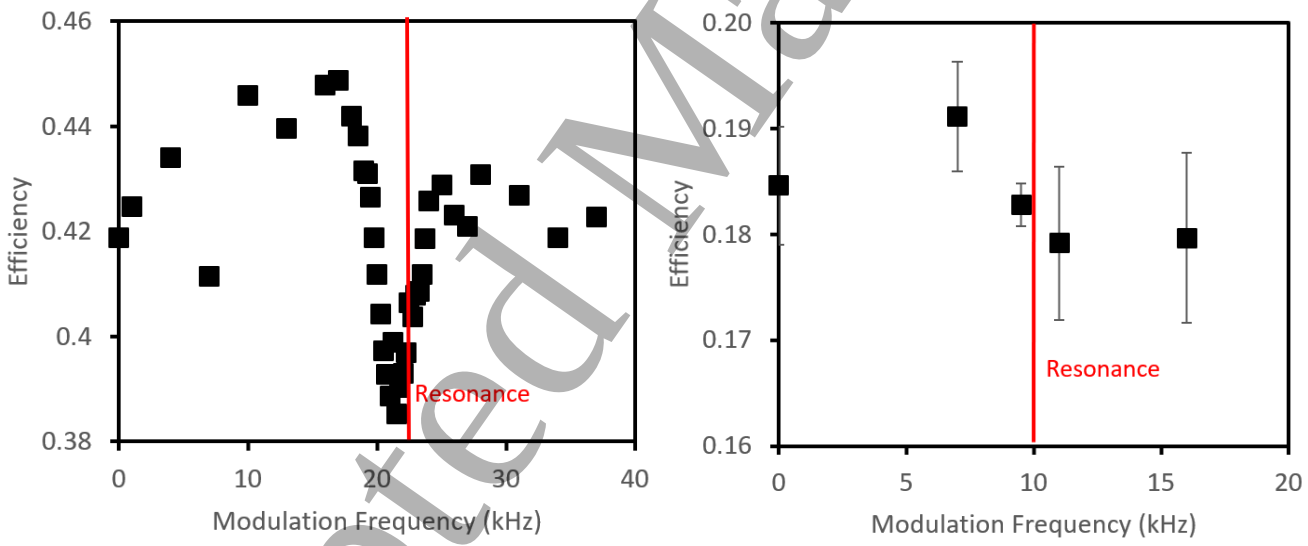

FIG A.3: Comparison of performance vs the modulation frequency for a Cylindrical Hall thruster with input voltage 220V and modulation amplitude ±40V for simulations (left) and experiments (right). Error bars of experimental thrust correspond to standard deviation over multiple measurements. The red line corresponds to the natural breathing frequency.

Appendix B. Error of Phase Measurements

Due to the entrainment of the modulation frequency with the discharge and ion current frequency near resonance, the measured phase angle between the ion energy and ion current (ion phase), and the phase angle between the anode voltage and the discharge current (discharge phase) was relatively consistent across all oscillations. Analysis of the entire spread of data revealed about 3° of standard error in the ion phase measurement near resonant frequencies (Fig. B.1). At frequencies further from the natural frequency of ~10 kHz, the standard error increased significantly: up to 25° for the ion phase at 20 kHz. This is likely due to the loss of entrainment as the natural frequency of the oscillations starts to dominate. It is notable that at these off-resonant frequencies the standard error in the ion phase was much worse than the discharge phase. This is likely to do with the technique used to measure the total ion current, which assumed entrainment of the oscillations (section 2.4).

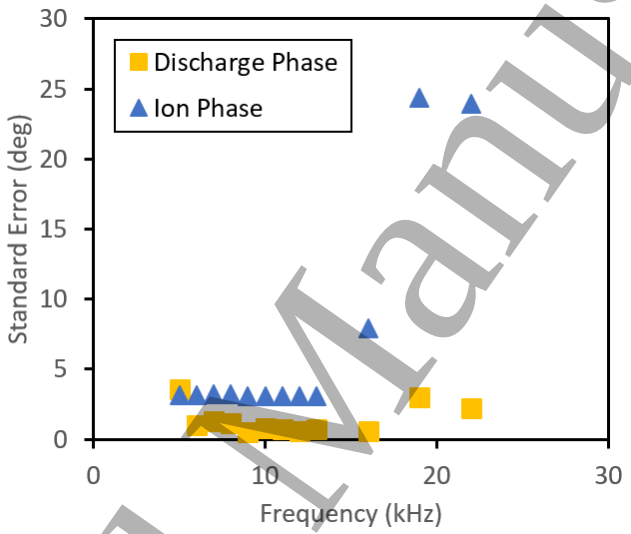

FIG B.1: Error of experimental discharge and ion phase measurements vs modulation frequency for a Cylindrical Hall thruster with input voltage 220V and modulation amplitude ±40V.

References

[1] Bouef J-P and Garrigues L 1998 Low frequency oscillations in a stationary plasma thruster *Journal of Applied Physics* **84**

[2] Fife J M 1998 *Hybrid-PIC modeling and electrostatic probe survey of Hall thrusters* (Massachusetts Institute of Technology)

[3] Hara K, Sekerak M J, Boyd I D and Gallimore A D 2014 Perturbation analysis of ionization oscillations in Hall effect thrusters *Phys. Plasmas* **21** 122103

[4] Raitses Y, Smirnov A and Fisch N J 2009 Effects of enhanced cathode electron emission on Hall thruster operation *Physics of Plasmas* **16** 057106

[5] Keller S, Raitses Y and Diallo A 2014 Driving Low Frequency Breathing Oscillations in a Hall Thruster *50th AIAA/ASME/SAE/ASEE Joint Propulsion Conference* 50th AIAA/ASME/SAE/ASEE Joint Propulsion Conference (Cleveland, OH: American Institute of Aeronautics and Astronautics)

[6] Hara K, Keller S and Raitses Y 2016 Measurements and theory of driven breathing oscillations in a Hall effect thruster *52nd AIAA/SAE/ASEE Joint Propulsion Conference* 52nd AIAA/SAE/ASEE Joint Propulsion Conference (Salt Lake City, UT: American Institute of Aeronautics and Astronautics)

[7] Romadanov I, Raitses Y, Diallo A, Kaganovich I, Hara K and Smolyakov A 2019 Time-resolved measurements of modulated breathing oscillations in Cylidnrical Hall Thruster *International Electric Propulsion Conference 2017* International Electric Propulsion Conference 2017 (Atlanta, Georgia)

[8] Romadanov I, Raitses Y and Smolyakov A 2019 Control of Coherent Structures via External Drive of the Breathing Mode *Plasma Phys. Rep.* **45** 134–46

[9] Romadanov I, Raitses Y and Smolyakov A 2018 Hall thruster operation with externally driven breathing mode oscillations *Plasma Sources Sci. Technol.* **27** 094006

[10] Wei L, Li W, Ding Y and Yu D 2018 Effect of low-frequency oscillation on performance of Hall thrusters *Plasma Sci. Technol.* **20** 075502

[11] Yamamoto N, Ito T, Takegahara H, Watanabe H, Tamida T and Osuga H 2016 Thrust Performance in Hall Thruster with Pulsating Operation *AEROSPACE TECHNOLOGY JAPAN* **14** Pb_173-Pb_176

[12] Yamamoto N, Takegahara H, Aoyagi J, Kuriki K, Tamida T and Osuga H 2015 Development of a Novel Power Processing Unit for Hall Thrusters *IEEE Trans. Plasma Sci.* **43** 158–64

[13] Tamida T, Osuga H, Yamamoto N, Takegahara H, Aoyagi J and Kuriki K 2015 Performance Improvement of Hall Thrusters Using a Pulse-Synchronous Driver System *Journal of Propulsion and Power* **31** 956–61

[14] Ellison C L, Raitses Y and Fisch N J 2012 Cross-field electron transport induced by a rotating spoke in a cylindrical Hall thruster *Physics of Plasmas* **19** 013503

[15] Raitses Y and Fisch N J 2001 Parametric investigations of a nonconventional Hall thruster *Physics of Plasmas* **8** 2579–86

[16] Simmonds J and Raitses Y Theoretical Analysis of Performance Parameters in Oscillating Plasma Thrusters *Journal of Propulsion and Power*

[17] Smirnov A, Raitses Y and Fisch N J 2002 Parametric investigation of miniaturized cylindrical and annular Hall thrusters *Journal of Applied Physics* **92** 5673–9

[18] Raitses Y, Gayoso J C and Fisch N J 2011 Effect of Magnetic Shielding on Plasma Plume of the Cylindrical Hall Thrusters *IEPC-2011-175* the 32nd International Electric Propulsion Conference (Wiesbaden, Germany)

[19] Raitses Y, Gayoso J C, Merino E and Fisch N 2010 Effect of the Magnetic Field on the Plasma Plume of the Cylindrical Hall Thruster with Permanent Magnets *46th AIAA/ASME/SAE/ASEE Joint Propulsion Conference & Exhibit* 46th AIAA/ASME/SAE/ASEE Joint Propulsion Conference & Exhibit (Nashville, TN: American Institute of Aeronautics and Astronautics)

[20] Granstedt E M, Raitses Y and Fisch N J 2008 Cathode effects in cylindrical Hall thrusters *Journal of Applied Physics* **104** 103302

[21] Smirnov A, Raitses Y and Fisch N J 2004 Plasma measurements in a 100 W cylindrical Hall thruster *Journal of Applied Physics* **95** 2283–92

[22] Staack D, Raitses Y and Fisch N J 2004 Temperature gradient in Hall thrusters *Appl. Phys. Lett.* **84** 3028–30

[23] Hofer R R, Jankovsky R S and Gallimore A D 2006 High-Specific Impulse Hall Thrusters, Part 1: Influence of Current Density and Magnetic Field *Journal of Propulsion and Power* **22** 721–31

[24] McVey J, Britt E, Engelman S, Gulczinski F, Beiting E, Pollard J and Cohen R 2003 Characteristics of the T-220 HT Hall-Effect Thruster *39th AIAA/ASME/SAE/ASEE Joint Propulsion Conference and Exhibit* 39th AIAA/ASME/SAE/ASEE Joint Propulsion Conference and Exhibit (Huntsville, Alabama: American Institute of Aeronautics and Astronautics)

[25] Raitses Y, Staack D, Dunaevsky A and Fisch N J 2006 Operation of a segmented Hall thruster with low-sputtering carbon-velvet electrodes *Journal of Applied Physics* **99** 036103

[26] Azziz Y 1979 *Experimental and Theoretical Characterization of a Hall Thruster Plume* (Massachusetts Institute of Technology)

[27] Raitses Y, Merino E, Parker J and Fisch N 2009 Operation and Plume Measurements of Miniaturized Cylindrical Hall Thrusters with Permanent Magnets *45th AIAA/ASME/SAE/ASEE Joint Propulsion Conference & Exhibit* 45th AIAA/ASME/SAE/ASEE Joint Propulsion Conference & Exhibit (Denver, Colorado: American Institute of Aeronautics and Astronautics)

[28] Goebel D M and Katz I 2008 *Fundamentals of electric propulsion: ion and Hall thrusters* (Hoboken, N.J: Wiley)

[29] Diamant K D, Pollard J E, Raitses Y and Fisch N J 2010 Ionization, Plume Properties, and Performance of Cylindrical Hall Thrusters *IEEE Trans. Plasma Sci.* **38** 1052–7

[30] Dunaevsky A, Raitses Y and Fisch N J 2006 Plasma acceleration from radio-frequency discharge in dielectric capillary *Appl. Phys. Lett.* **88** 251502

[31] Kolbeck J, Porter T and Keidar M 2017 High Precision Thrust Balance Development at the George Washington University *International Electric Propulsion Conference 2017* International Electric Propulsion Conference 2017 (Atlanta, Georgia)

[32] Simmonds J B, Raitses Y, Smolyakov A, Chapurin O and Chaplin V H 2020 Application of Hall Thrusters with Modulated Oscillations *AIAA Propulsion and Energy 2020 Forum* AIAA Propulsion and Energy 2020 Forum (VIRTUAL EVENT: American Institute of Aeronautics and Astronautics)

[33] Hagelaar G J M, Bareilles J, Garrigues L and Boeuf J-P 2004 Modelling of Stationary Plasma Thrusters *Contrib. Plasma Phys.* **44** 529–35

[34] Boeuf J-P 2017 Tutorial: Physics and modeling of Hall thrusters *Journal of Applied Physics* **121** 011101

[35] Hagelaar G J M, Bareilles J, Garrigues L and Boeuf J-P 2002 Two-dimensional model of a stationary plasma thruster *Journal of Applied Physics* **91** 5592–8

[36] Garrigues L, Hagelaar G J M, Bareilles J, Boniface C and Boeuf J P 2003 Model study of the influence of the magnetic field configuration on the performance and lifetime of a Hall thruster *Physics of Plasmas* **10** 4886–92

[37] Bareilles J, Hagelaar G J M, Garrigues L, Boniface C, Boeuf J P and Gascon N 2004 Critical assessment of a two-dimensional hybrid Hall thruster model: Comparisons with experiments *Physics of Plasmas* **11** 3035–46

[38] Hagelaar G J M, Bareilles J, Garrigues L and Boeuf J-P 2003 Role of anomalous electron transport in a stationary plasma thruster simulation *Journal of Applied Physics* **93** 67–75

[39] Smolyakov A, Chapurin O, Romadanov I, Raitses Y and Kaganovich I 2019 Theory and Modelling of Axial Mode Oscillations in Hall Thruster *AIAA Propulsion and Energy 2019 Forum* AIAA Propulsion and Energy 2019 Forum (Indianapolis, IN: American Institute of Aeronautics and Astronautics)

[40] Diallo A, Keller S, Shi Y, Raitses Y and Mazouffre S 2015 Time-resolved ion velocity distribution in a cylindrical Hall thruster: Heterodyne-based experiment and modeling *Review of Scientific Instruments* **86** 033506

[41] Young C V, Fabris A L, MacDonald-Tenenbaum N A, Hargus W A and Cappelli M A 2018 Time-resolved laser-induced fluorescence diagnostics for electric propulsion and their application to breathing mode dynamics *Plasma Sources Sci. Technol.* **27** 094004

[42] Dale E T and Jorns B A 2019 Non-invasive time-resolved measurements of anomalous collision frequency in a Hall thruster *Physics of Plasmas* **26** 013516

[43] Smirnov A, Raitses Y and Fisch N J 2004 Electron cross-field transport in a low power cylindrical Hall thruster *Physics of Plasmas* **11** 4922–33